Eur. Phys. J. C 26, 3–7 (2002)
Digital Object Identifier (DOI) 10.1140/epjc/s2002-01060-y

THE EUROPEAN PHYSICAL JOURNAL C

Application of wavelet analysis to the spectrum of ω' states and ratio $R_{e^+e^-}$

V.K. Henner[1,2,a], P.G. Frick[3], T.S. Belozerova[1], V.G. Solovyev[2]

[1] Department of Theoretical Physics, Perm State University, 614600 Perm, Russia,
[2] Department of Physics, University of Louisville, Louisville, KY 40292, USA
[3] Institute of Continuous Media Mechanics, 614013 Perm, Russia

Received: 4 February 2002 / Revised version: 28 August 2002 /
Published online: 18 October 2002 –

Abstract. We demonstrate the advantages of the wavelet analysis (WA) for resolving the structures in experimental data on e^+e^- annihilation into hadron states with quantum numbers of ω meson. The WA yields a useful set of starting conditions for analysis of ω' states with multiresonance unitary Breit-Wigner method. We also apply the WA for the ratio $R_{e^+e^-}$.

1 Introduction

The e^+e^- annihilation experimental data provide several vector states above 1 GeV. The properties of these states and even their number are not well established. The main difficulties encountered in understanding the situation are large statistical errors in the data and overlapping of these states decaying into several final channels. In such situations it is important to resolve structures in the data before applying any method based on some physical assumptions. It is also important that a description of the partial wave amplitudes preserves unitarity when resonances r_i with the same quantum numbers overlap, i.e. $\mid E_{r_i} - E_{r_j} \mid \sim \Gamma_{r_i} + \Gamma_{r_j}$.

We use the wavelet analysis for structure recognition of the data. It is often said that the WA works like a "microscope" differentiating between a variety of scales - both the characteristic scales and the positions of any local structures are obtained independently of the general structure of the data. The wavelet transform smooths out the experimental data before going into theoretical analysis i.e., it suppresses statistical noise picking out signals that would otherwise be obscured. The method is commonly used in image and signal processing, and can be also of considerable interest in the context of experimental particle and nuclear physics.

The plan of this paper is as follows. In Sect. 2 a brief discussion of the wavelets is presented. Section 3 gives an example of the WA of ω' states in e^+e^- annihilation. The wavelet analyzed data are used as an input to study the partial wave amplitudes. The application of the WA for "smearing" the ratio $R_{e^+e^-}$ is presented in conclusion.

[a] e-mail: vhenner@python.physics.louisville.edu and henner@psu.ru

2 Wavelets and structure recognition

The wavelets can efficiently detect essential structures in data sets in a wide range of scales (for example, see the books of Holschneider [1] or Torresani [2]). Before giving a very brief description of WA, we would like to note that we are not the only ones performing a kind of data "optimization" in elementary particle physics. To be more specific let us draw the analogy between this work and the works on "optimization" of the ratio $R_{e^+e^-}$ in QCD [3–5]. The data on $R_{e^+e^-}$ have a wide range of structures and large statistical errors, making a direct comparison with QCD highly impossible. However, a meaningful comparison can be made provided that some kind of "smearing" procedure is used. The smeared ratio

$$\bar{R}_{e^+e^-}(s,\Delta) = \frac{\Delta}{\pi}\int\limits_0^{s_{max}} \frac{R_{e^+e^-}(s')}{(s'-s)^2+\Delta^2}ds' \qquad (1)$$

was introduced [3] to smooth out any rapid variations in $R_{e^+e^-}$.

The difference between the described procedure and the analysis to be used for determining resonance parameters is that compared to "smearing" we need to resolve the structures and, what is more important, we need to reveal structures corresponding to different scales ("global" and local). In this sense, the WA seems to be the most appropriate means for achieving this purpose. In Sect. 4 we will return to the discussion of the ratio $R_{e^+e^-}$ to demonstrate that the WA provides a very reasonable and simple way of its "smearing".

Over the past few years WA has steadily gained favor in different areas of physics. Therefore it seems to be rather strange that it is poorly known in the particle and nuclear physics even though it can be readily extended

for studying energy scaling of the data. It was successfully applied to the processes of multiple production, as demonstrated by references in reviews [6], and for studying the angular distributions of secondary particles [7] (see also our analysis of ρ' states [8]).

A continuous wavelet transformation of the function $f(t)$ (the data) is defined as:

$$w(a,t) = C_\psi^{-\frac{1}{2}} a^{-\frac{1}{2}} \int_{-\infty}^{+\infty} \psi^* \left(\frac{t'-t}{a} \right) f(t') dt', \qquad (2)$$

where a constant C_ψ is obtained in terms of Fourier transformation of $\psi(t)$:

$$C_\psi = \int_{-\infty}^{+\infty} |\omega^{-1}| |\hat{\psi}(\omega)|^2 d\omega \ , \ \ \hat{\psi}(\omega) = \int_{-\infty}^{+\infty} \psi(t) e^{-i\omega t} dt. \quad (3)$$

Here, as in most relevant literature, an argument t is referred to as "time", even though in our actual problem it is an energy variable. Decomposition (2) is performed by convolution of the function $f(t)$ with a biparametric family of self-similar functions generated by dilatation and translation of the analyzing function $\psi(t)$, called wavelet:

$$\psi_{a,b}(t) = \psi \left(\frac{t-b}{a} \right), \qquad (4)$$

where the scale parameter a characterizes the dilatation, and b characterizes the translation in time or space. It is a kind of "window function" with non-constant window's width: high frequency wavelets are narrow (due to the factor $1/a$), while low frequency wavelets are much broader. The function $\psi(t)$ should be well localized in both time and Fourier spaces and must obey the admissibility condition, $\int_{-\infty}^{+\infty} \psi(t) dt = 0$. This condition requires that ψ must be an oscillatory (but with the limited support) function and, if the integrals (3) converge, the completeness of the wavelet functions provides the existence of inverse transformation:

$$f(t) = C_\psi^{-\frac{1}{2}} \int_{-\infty}^{+\infty} \int_{0}^{+\infty} \psi \left(\frac{t-t'}{a} \right) w(a,t') \frac{dt'da}{a^{5/2}} \ . \qquad (5)$$

The wavelets with a good localization in physical space and with a small number of oscillation are commonly used to recognize the local features of data, and to find the parameters of dominating structures (location and scale/ width). In this work, we use one of the most popular wavelets of this type, the so-called 'Mexican Hat'(MH) function

$$\psi(t) = (1-t^2) e^{-t^2/2}. \qquad (6)$$

A very helpful representation of the WT revealing the whole spectrum of the signal features is the "time-frequency" plane. This is a multiresolution spectrogram, which shows the frequency (scale) contents of the signal as a function of time. Each pixel on the spectrogram represents $w(a,t)$ for a particular a (scale) and t (time). The location of spots on the vertical axis (scale axis, a) corresponds to the width of the maximum. The intensity of dark spots shows the amplitudes of maxima. The noise is located at the bottom of the wavelet plane (small scale regions, or high frequencies). In order to separate the signal from the background noise, the wavelet reconstruction is performed for scales (scale parameter values) greater than a certain scale a_{noise}, which will be termed the boundary (or cut-off) scale. In deciding on the appropriate boundary scale that will separate the noise-like high frequency components of data we hold to a pragmatic line of reasoning: the best option of a_{noise} is the smallest one, which will smooth out any rapid variations in data and enable us to reproduce stable results for low frequencies (resonance area). A similar pragmatic strategy was applied in [3,4] to choose the parameter Δ that should be reasonably high to compare the smeared $\bar{R}_{e^+e^-}$ with QCD models, but not too large to be able to keep some fine details of the data.

The reconstructed data are obtained using the inverse transformation (5)

$$f_r(t) = < f > + C_\psi^{-\frac{1}{2}} \int_{a_{noise}}^{a_{max}} \int_{t_{min}}^{t_{max}} \psi_{a,t}(t') w(a,t') \frac{dt'da}{a^{5/2}} \ . \quad (7)$$

The $< f >$ must be added to the reconstructed signal to restore the mean value of the original signal (the mean value of the WT is zero because an average value of any wavelet is zero). Formula (7) in the limit $a_{noise} \to 0$, $a_{max} \to \infty, t_{min} \to -\infty, t_{max} \to +\infty$ is equivalent to exact relation (5), but in practice a limited number of experimental points on the restricted energy interval leads to a limited domain in the integral (7). To fill in the gaps between the experimental points we use a linear interpolation. In practice, different interpolations lead to a small difference in the restored signal (which gives a very small difference on a lower part of the wavelet plane corresponding to noise). Note also that one of the advantages of the WA is a fairly low sensitivity of the restored signal to any physically reasonable continuation of the "data" outside the interval (t_{min}, t_{max}) where the data are known.

3 ω' states: Combined wavelet and BW analysis

The analysis was performed for ρ' and ω' states but for the sake of clarity we present the case of ω' states only (it involves a smaller number of states and channels than those related with the ρ' states).

The wavelet planes shown in Figs. 1 and 2 for the processes $e^+e^- \to \pi^+\pi^-\pi^0$ [9,10], and $e^+e^- \to \omega\pi\pi$ [11] clearly display two ω' states approximately at 1.4 and 1.6 GeV. The wavelet transformation images obtained with the MH wavelet are shown at the top of the diagrams. The WT localizes the structures in a fashion that allows us to

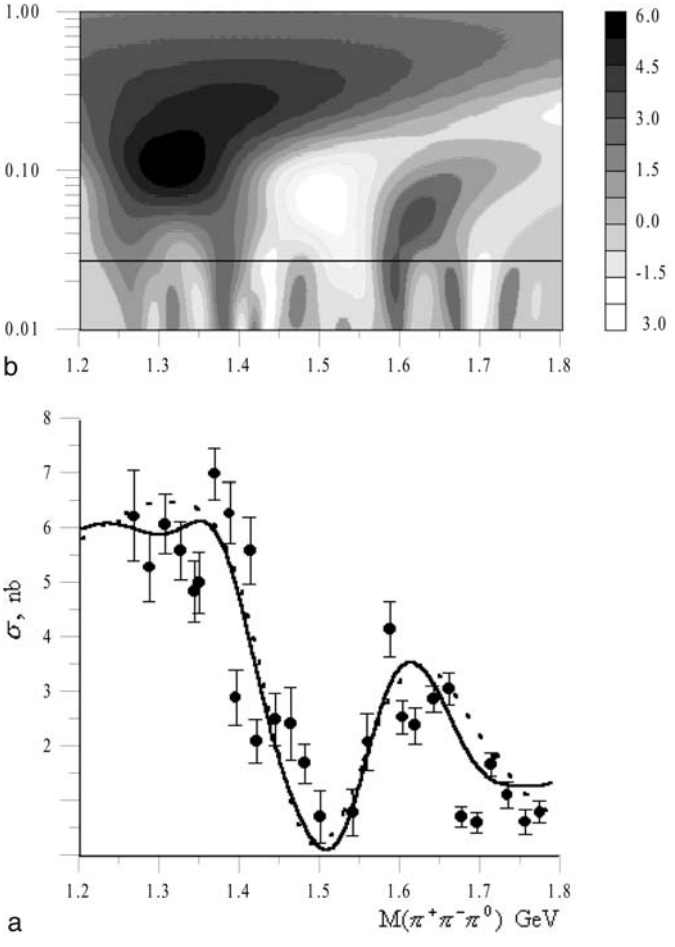

Fig. 1a,b. Cross-section $e^+e^- \to \pi^+\pi^-\pi^0$

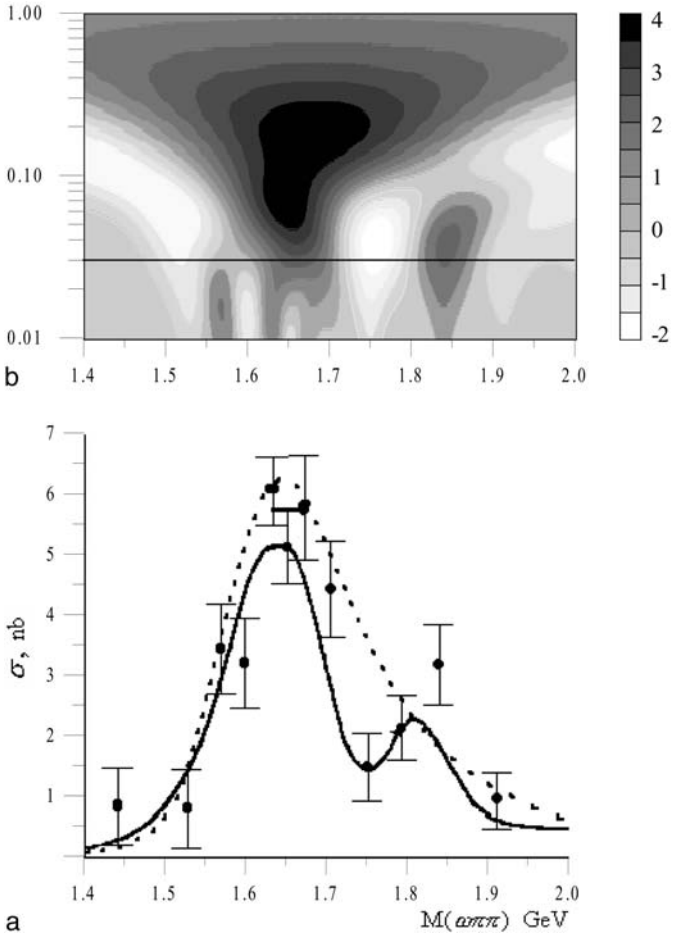

Fig. 2a,b. Cross-section $e^+e^- \to \omega\pi\pi$

estimate the masses of the resonances and their widths. The straight horizontal lines correspond to the boundary scale a_{noise} which cuts off the small scale structures. The curves in the figures represent reconstructed data obtained by the inverse transformation technique(7). A spot in Fig. 2b at 1.85 GeV indicates one more possible state, but the location of this spot along the vertical axis shows that this state is sensitive to the cut-off value a_{noise}.

Due to overlapping, the observed positions of maxima can differ from the physical resonance masses, and partial and total widths can essentially differ from preliminary estimations. Coherent fitting of amplitudes in a proper partial wave analysis (in unitary BW analysis for simpler cases) may be better suited. The WA in this case yields a useful set of starting conditions for a more accurate analysis.

The interference of the resonances with the same decay channels is the key aspect of any analysis and interpretation. In the Breit-Wigner (BW) approach this interference is often taken into account by relative phases in BW terms, which are treated as free parameters, the most common choices being 0 or π. The results of analysis critically depend on the choice of the phase set. Whether these phases are included or not, such a sum of BW terms looses unitarity, which is the basic point in the BW description.

There are several approaches preserving unitarity, for example an often used K-matrix method. Contrary to this approach, the BW method directly provides the physical parameters of the resonances, their masses, widths and branching fractions.

Let us briefly formulate BW method preserving unitarity (details and relation to different methods are described in [12,13]). Let the partial wave amplitudes be written as

$$f_{ij}(s) = \sum_{r=1}^{N} \frac{m_r \Gamma_r g_{ri} g_{rj}}{s - m_r^2 + i m_r \Gamma_r} = \sum_{r=1}^{N} e^{i(\varphi_{ri}+\varphi_{rj})} \frac{m_r \Gamma_r \mid g_{ri} \mid\mid g_{rj} \mid}{s - m_r^2 + i m_r \Gamma_r} , \qquad (8)$$

where the energy independent relative phases φ_{ri} are not free parameters but should be determined in such a way as to preserve unitarity (note, that the number of free parameters is smaller than or equal to that in a "naive" BW or K matrix approach). Here we employ an approximation of energy independent widths, which is commonly used for vector states. Index $i = 1$ corresponds to the initial state e^+e^- (or to the virtual photon), index $j = 2, 3$ corresponds to the final states $\rho\pi$ and $\omega\pi\pi$ (which are the two main channels of the ω' states decay [14]), index r

Table 1. Parameters of the ω' states (in GeV)

Meson	Mass	Width
ω'_1	1.450 ± 0.010	0.199 ± 0.015
ω'_2	1.619 ± 0.005	0.250 ± 0.014

Table 2. Branching ratios of the ω' states (in %)

State	ω'_1	ω'_2
e^+e^-	$(23 \pm 1.0)10^{-5}$	$(32 \pm 1.0)10^{-5}$
$\rho\pi$	69.92 ± 2.85	38.03 ± 1.37
$\omega\pi\pi$	30.08 ± 2.85	61.97 ± 1.36

enumerates two ω' states ($\omega - \phi$ contribution is included), g_{ri} are coupling constants.

A comparison of the reconstructed signals and expression (8) gives a good fit with χ^2/n_D of about 1.3. In Figs. 1 and 2 reconstruction is shown by a solid line, and fit by a dotted line. (Experimental data [11] are multiplied by the factor 1.5 to include unobserved $\omega\pi^0\pi^0$ state.) Starting from the WA masses (and widths) we allow large deviations of about 150 MeV from these positions in either direction. The masses and widths are listed in Table 1, the branching ratios are listed in Table 2 (the leptonic width obtained from this table are $\Gamma_{\omega'_1\to e^+e^-} \approx 0.46keV$ and $\Gamma_{\omega'_2\to e^+e^-} \approx 0.80keV$). The error bars for the resulting parameters have been derived as the square roots of the diagonal elements of the covariance matrix of parameters' estimations. All the parameters are in good agreement with PDG review [14].

4 Conclusion

Numerous applications of wavelets to data analysis in different fields of mathematics and physics have proved them to be a powerful tool for studying the fractal data. This technique can be successfully applied to some problems of nuclear and high-energy physics where the wavelet analysis will work as a tool for studying energy scaling of the process.

We performed the WA of the data in order to clear out the resonance contribution. Due to good scaling properties of the wavelets we can consider the data with various resolution which allows us to separate the resonances from noise and from each other. Such a local analysis (and the corresponding reconstruction) is very significant when it is necessary to distinguish between several resonances in the data with large errors.

The WA shows that some experimental data are statistically inadequate in the sense that they do not allow separation of the noise contribution. This fact emphasizes an apparent virtue of the method which provides criteria for distinguishing between "stable" and "unstable" data - the latter do not reproduce the same essential structures when the contribution of the experimental noise changes slightly. Technically it means that the structure (resonance) is questionable if it is sensitive to the noise cut-off value. Interestingly, this criterion supports ρ' and ω' states at about 1.45 and $1.65-1.70$ GeV in accord with the summary paper on vector mesons [14] that includes only these states as reliably established. We obtained the parameters of these two ω' states by applying the BW unitary method to the wavelet analyzed data, and they agree fairly well with those in [14]. The only conclusion suggesting itself from WA about the states differing from these two states is that their existence is consistent with the experimental data, although the cross sections measurement accuracy should be improved.

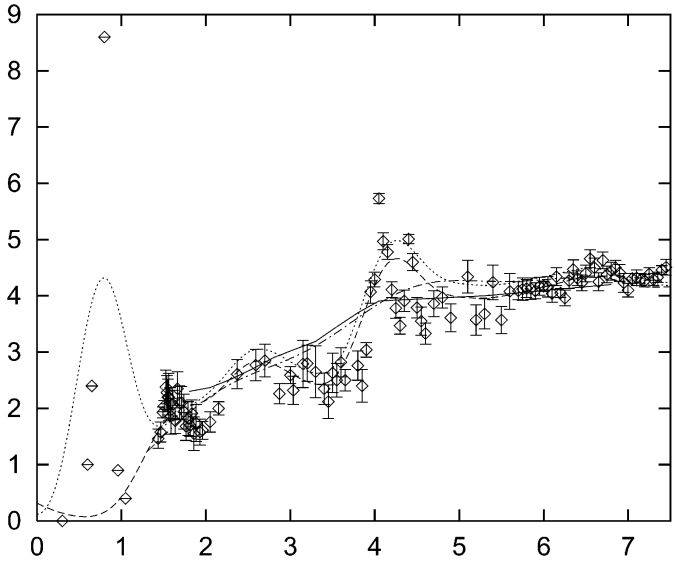

Fig. 3. Ratio $R_{e^+e^-}$

To conclude this paper, let us return to the ratio $R_{e^+e^-}$ to demonstrate another application of the wavelet technique to high-energy physics. To smooth out any rapid variations in $R_{e^+e^-}$ we may remove high frequency noise with WT, which provides a smearing alternative to the procedure (1). The wavelet approach is ideally suited for this purpose because of its multiscale nature. The restored data in the Fig. 3 (experimental points are from [14]) keep all main features of $R_{e^+e^-}$ with statistical errors and threshold singularities damped, which allows a direct comparison with the corresponding QCD smeared quantity. The stability of restored data at fairly large variations of the cut-off scale reflects the quality of the $R_{e^+e^-}$ data.

We restored the $R_{e^+e^-}$ on the same interval as in the works [3,4], from about 1.4 to 7.5 GeV. It is interesting to compare how the resonances and $E < 1.4$ and $E > 7.5$ GeV regions have been treated in [3,4] and in our approach. With the approach developed in [3] it was necessary to exclude the sharp resonances, ψ, ψ', etc. from the data to calculate the integral (1). Moreover, it was necessary to exclude a rather wide ρ peak that substantially contributes to (1). Then a term was added to account for the contribution from s_{max} to ∞, assuming that $R_{e^+e^-}$ remains constant above $s_{max} \approx 60GeV^2$. Originally, the smearing procedure [3] supposes a global constant value of Δ in (1) (in [3] a value $\Delta = 3GeV^2$ was used). How-

ever it was found out [4] that for different energy regions it would be better to use different values of Δ. Note, that using of energy dependent Δ in (1) in some sense reflects the necessity of using different scales. With the WA approach there is no need to remove the resonances by hand - the sharp resonances are getting just a part of high frequency noise background and the ρ meson contribution in the smeared $R_{e^+e^-}$ is possible to evaluate. Above 1.5 GeV, for a large cut-off value a_{noise}, the ρ meson contribution just gives some small vertical shift for the restored curve - the dotted curve on the Fig. 3 is obtained by including all experimental points above $2m_\pi$ threshold, and the dashed curve is obtained when the data from the threshold were continued to the first on the figure's experimental point at about 1.4 GeV using a linear approximation (thus excluding the ρ peak). When the cut-off value a_{noise} is increasing, the difference between these two curves becomes very small - the corresponding reconstructed data for the value $a_{noise} = 0.6$ are represented by the dashed-dotted line. The contribution of the interval well beyond 8 GeV (we use the data from [14] up to 60 GeV) to the restored data is negligible below 8 GeV. Any continuations used above 60 GeV contribute nothing. As seen in Fig. 3, our WA smeared ratio $R_{e^+e^-}$ is in good agreement with the theoretical prediction (solid line, [5]) for QCD smeared ratio.

Acknowledgements. We thank D.V.Shirkov for attracting attention to smearing of the ratio $R_{e^+e^-}$, and thus inspiring the application of the WA to that ratio, and S.B.Gerasimov and K.Forinash for very useful discussions. The research described in this publication was made possible in part by Award No. PE-009-0 of the U.S. Civilian Research & Development Foundation for the Independent States of the Former Soviet Union (CRDF).

References

1. M. Holschneider, Wavelets: An analysis tool, (Oxford University Press, 1995)
2. B. Torresani, Analyse continue par ondelettes. Savoirs actuels (1995)
3. E.C. Poggio, H.R. Quinn, S. Weinberg, Phys.Rev.D **13**, 1958 (1976)
4. A.C. Mattingly, P.M. Stevenson, Phys.Rev.D **49**, 437 (1994)
5. I.L. Solovtsov, D.V. Shirkov, Teor.Math.Fiz. **120**, 1220 (1999)
6. I.M. Dremin, Usp. Fiz. Nauk, **170**, 1235 (2000); I.M. Dremin, O.V. Ivanov, V.A. Nechitailo, Usp. Fiz. Nauk, **171**, 465 (2001)
7. S. Afanasiev, M. Altaisky, Yu. Zhestkov, Nuovo Cimento A**108**, 919 (1995)
8. V.K. Henner, P.G. Frick, T.S. Belozerova, in Proceedings of the 9th Int. Conf. Hadron 2001, IHEP, Protvino (2001); in Proceedings of the 9th Int. Conf. Baryons 2002, Jefferson Lab (2002)
9. V.M. Aulchenko, et al., Preprint INP-86-106, Novosibirsk (1986)
10. Baldini-Ferroli, in Proc. Had. Phys. at intermediate Energy, Elsevier (1987)
11. A. Cordier, et al., Phys.Lett.B **106**, 155 (1981)
12. T.S. Belozerova, V.K. Henner, Physics of Particles and Nuclei **29**, 63 (1998)
13. V.K. Henner, T.S. Belozerova, Yad.Fizika **60**, 1998 (1997); **61**, 127 (1998)
14. D.E. Groom, et al., Eur.Phys.J. C **15**, 1 (2000)